

Title:

Polarization-independent tunable optical filters based on liquid crystal polarization gratings

Authors:

Elena Nicolescu and Michael J. Escuti

Affiliation:

North Carolina State University, Dept Electrical & Computer Engineering, Raleigh, NC (USA)

Presented At:

SPIE Optics & Photonics Conference, San Diego, CA (August 26, 2007)

Citation:

E. Nicolescu and M.J. Escuti, "Polarization-independent tunable optical filters based on liquid crystal polarization gratings", *Proceedings of SPIE*, vol. **6654**, no. 665405 (2007).

Copyright 2007 Society of Photo-Optical Instrumentation Engineers.

This paper was published in Proceedings of SPIE Vol. 6654 and is made available as an electronic reprint with permission of SPIE. One print or electronic copy may be made for personal use only. Systematic or multiple reproduction, distribution to multiple locations via electronic or other means, duplication of any material in this paper for a fee or for commercial purposes, or modification of the content of this paper are prohibited.

Polarization-independent tunable optical filters based on liquid crystal polarization gratings

Elena Nicolescu and Michael J. Escuti

North Carolina State Univ, Dept Electrical & Computer Engineering, Raleigh, NC (USA)

ABSTRACT

We introduce and demonstrate a novel tunable optical filter that is insensitive to input polarization. While the most obvious application of this novel filter is in compact spectroscopy, all technologies that are dependent on tunable passband filters can benefit from it. Analogous to Lyot and Solc filters, this filter is constructed of multiple liquid crystal polarization gratings (LCPGs) of different thicknesses. LCPGs are switchable, anisotropic, thin diffraction gratings which exhibit unique properties including diffraction at visible and infrared wavelengths that can be coupled between only the zero- and first-orders, with nearly 100% and 0% experimentally verified efficiencies. Most relevant to the filter concept introduced in this work, the transmittance of the LCPG zeroth order is independent of the incident polarization. When combined with an elemental spatial filter, polarization-independent bandpass tuning can be achieved with minimum loss. The unique filter design enables a high peak transmittance ($\sim 90\%$) that is difficult in competing polarizer-based technologies. In this work we derive the core principles of the tunable filter, present preliminary experimental data, and discuss the capabilities of the filter in terms of finesse, 3dB bandwidth (full-width at half-maximum), and free-spectral-range. We will also evaluate the most likely practical limitations imposed by material properties and fabrication.

Keywords: liquid crystals, tunable optical filter, bandpass, polarization gratings, diffraction, polarization-independent

1. INTRODUCTION

The applications of tunable optical filters range from spectroscopy to optical communication networks to biomedical imaging. The most successful approaches include dispersive elements matched with aperture-stops (Czerny-Turner), mechanically tuned etalons (Fabry-Perot), and assemblies of stacked birefringent waveplates and polarizers (Lyot, Solc, and Evans). Despite their popularity, these designs are in many contexts costly to implement, may have high insertion losses, manifest strong polarization sensitivity, or are difficult to miniaturize into a physically small package. In this work we describe, analyze, and demonstrate a tunable filter based on stacked Liquid Crystal Polarization Gratings (LCPGs) which exhibits complete polarization-independence, high peak transmittance ($\sim 90\%$), and potential for very low cost implementation. We will first introduce the relevant properties of single LCPGs and describe the behavior of multiple stacked LCPGs configured as a tunable bandpass filter. We will explore different design options and their tradeoffs, and present preliminary experimental data.

2. BACKGROUND

Of the various birefringent filters introduced over the past several decades, many are derived from the Lyot-Ohman filter.¹ The Lyot-Ohman filter, whose main advantage is achieving very narrow passbands, is composed of a series of stacked birefringent plates that are separated by polarizers, where tuning is accomplished simply by rotating the birefringent plates.² However, it requires the use of many polarizers resulting in low transmittance and a high polarization-sensitivity. In an effort to improve upon the Lyot-Ohman design, Solc³⁻⁵ filters were developed with the same basic principle of operation but differing configurations of retarders and polarizers. While the Solc design requires fewer polarizers (increasing peak transmission), it has a significantly larger passbands.⁶ The Evans⁷ filters were developed as a compromise between these two designs. Beyond the family of tunable birefringent layer filter approaches, it is important to note that other designs such as the Fabry-Perot

Correspondence should be addressed to: mjescuti@ncsu.edu, +1 919 513 7363

etalon filter have also been successfully implemented. These designs use variable-length resonant cavities to achieve tunability and have been successfully implemented recently using MEMS technologies.⁸ While these devices boast wide tunability, they are comparatively costly to implement and nevertheless usually demand careful polarization management.

The integration of liquid crystal (LC) technology into tunable optical filters has successfully improved performance, power requirement, and manufacturing cost. In order to improve tunability in Lyot type systems, the traditional birefringent plates can be replaced with a series of LC fixed and tunable retarders.^{6,9} This allows the effective LC birefringence to be controlled electrically (instead of mechanically). LC-based Fabry-Perot etalon filters have achieved non-mechanical tunability by filling the etalon cavity with LC material.¹⁰ A reduced polarization dependence has also been achieved by the addition of birefringent quarter waveplates¹¹ in an optical fiber-based scheme.

LC tunable reflection filters have also been demonstrated by manipulating the unique properties of chiral LCs. For instance, in chiral nematics, an electric field applied perpendicular to the helical axis can deform the cholesteric pitch and shift the reflected wavelength.¹² While this approach avoids polarizers, it only operates on a single circular polarization handedness and its passband peak reflectance has an inherently strong voltage-dependency. In an alternative approach, a vertically-aligned deformed-helix ferroelectric LC can be configured so that a reflective notch filter (via a Bragg effect) can be tuned by temperature¹³ and applied voltage.¹⁴ This results in a polarization-independent effect over a wide range, but its notch depth appears limited and has a peak reflectance that is also inherently voltage-dependent.

The tunable filter design discussed in this paper is analogous to Lyot-Ohman and Solc filters in that it is composed of several birefringent layers. However, unlike its predecessors, this design is based on diffraction and is completely independent to the polarization state of the input. We rely on the properties of nematic LC under the influence of a predetermined alignment pattern and an applied electric field. The design exhibits low insertion losses, uses no polarizers, and shows strong potential for minimized cost and small packaging. These characteristics make the filter highly suitable for integration into a compact spectrometer system, which we have designed, implemented, and analyzed in a parallel study.¹⁵

3. LIQUID CRYSTAL POLARIZATION GRATING BASICS

The basic component of our filter assembly is the liquid crystal polarization grating (LCPG), a switchable, anisotropic, diffraction grating actively being developed for many applications, including high-efficiency microdisplays,^{16,17} hyperspectral polarimetry,¹⁸ and generic diffractive optical elements.^{19–22} Here we show how they can be configured to achieve a compelling polarization-independent tunable optical filter.

Polarization gratings^{23,24} (PGs), sometimes called anisotropic or vectorial gratings, are embodied as a spatially varying birefringence and/or dichroism, and essentially operate by periodically modulating the polarization state of the wavefront passing through them (as opposed to modulating phase or amplitude alone). One of the most important PG profiles is a continuous, in-plane, linear birefringence texture^{23–25} with a uniaxial optical anisotropy that follows the spatial profile $\mathbf{n}(x) = [\sin(\pi x/\Lambda), \cos(\pi x/\Lambda), 0]$, where Λ is the grating period. An effective way^{16,19,26} to create this is using bulk nematic LCs aligned by photo-alignment surfaces that have been exposed with a polarization hologram, leading to the structure illustrated in Fig. 1(a) and (b) where the linear birefringence is embodied in a nematic director $\mathbf{n}(x)$. Note that the key parameters of an LCPG (Fig. 1) include the grating period Λ , grating thickness d , linear birefringence Δn , average index \bar{n} , and voltage threshold V_{th} .

Diffraction from this elegant structure is somewhat surprising and broadly useful. Assuming the grating parameter²⁷ $\rho < 2\lambda^2/\bar{n}\Delta n\Lambda^2$, we can express the relevant diffraction efficiency^{18,23} for light normally incident (within $\pm 20^\circ$):

$$\eta_0(\lambda) = \cos^2\left(\frac{\pi\Delta nd}{\lambda}\right) \quad (1)$$

where η_0 is the zero-order diffraction efficiency and λ is the vacuum wavelength of incident light. Graphed in Fig. 1(d) using representative parameters ($\Delta n = 0.2$ and $d = 7 \mu\text{m}$), several notable aspects can be observed: (i) it can theoretically vary from 100% to 0% depending on the retardation $\Delta nd/\lambda$; (ii) the specular transmitted intensity is independent of input polarization and Λ ; (iii) peak zero-order efficiencies occur at wavelength $\lambda_N =$

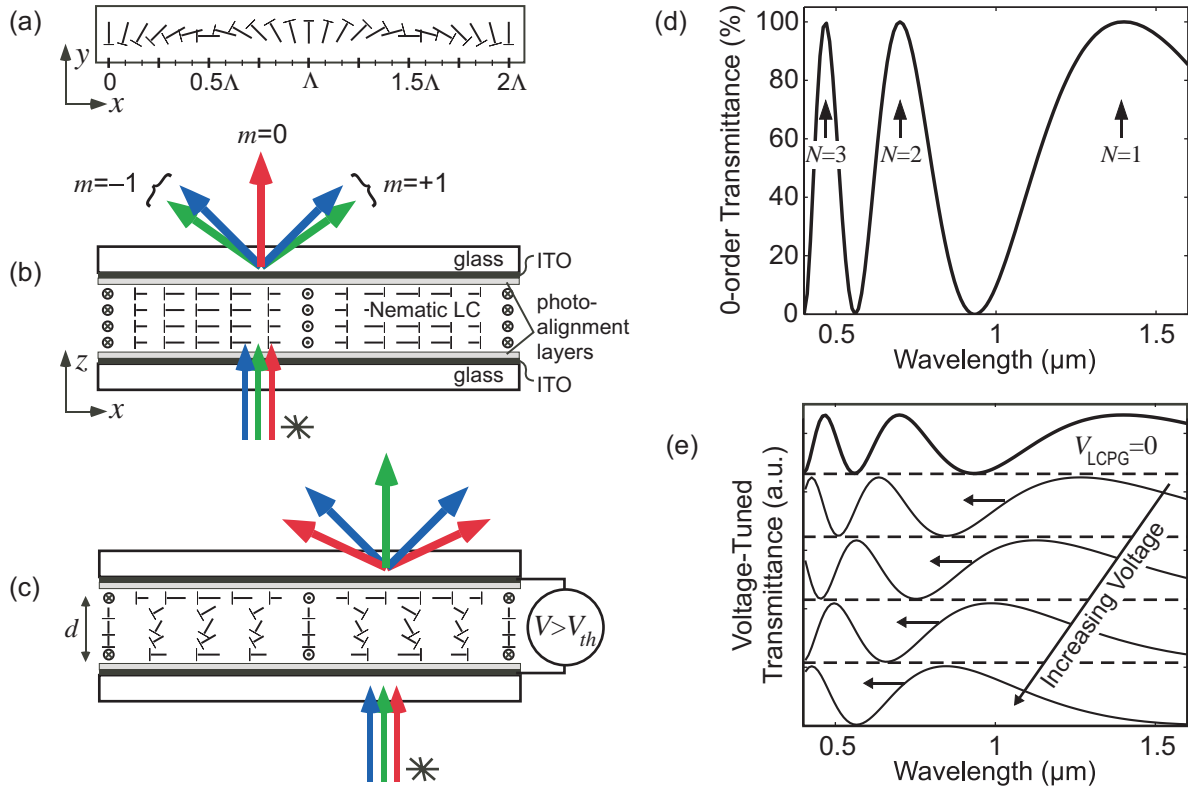


Figure 1. Structure and properties of the liquid crystal polarization grating (LCPG): (a) Basic geometry (top view); (b) Basic geometry (side view) and illustrated diffraction behavior when $\Delta nd =$ red wavelength with zero applied voltage - note that only the ± 1 -orders are ideally present regardless of input polarization; (c) Diffraction behavior when the applied voltage exceeds V_{th} - note that light at different wavelengths couple into the zero-order; (d) Example spectrum ($\Delta n = 0.2$, $d = 7 \mu\text{m}$) shows multiple spectral fringes N over the visible and near-infrared range; and (e) Effect of applied voltage V_{LCPG} on spectrum is a blue-shift. Note that illustrations are not drawn to scale. (color figure)

$\Delta nd/N$, where N is a non-negative integer corresponding to the spectral fringe; and conversely, (iv) the thickness required to arrange a fringe N at a wavelength λ_N obeys the rule

$$d = N\lambda_N/\Delta n. \quad (2)$$

Electrical control of the diffraction efficiency occurs by decreasing the effective birefringence (in fact, $\Delta n \rightarrow \Delta n(V)$ should be substituted in Eq. (1)). As an external voltage V is applied (Fig. 1(c)), the nematic director reversibly reorients out-of-plane, thereby leading to a blue-shift in the entire spectrum (Fig. 1(e)). As an illustrated example, if the product Δnd is set so that red light is transmitted when $V = 0$ and lower wavelengths are predominantly diffracted (Fig. 1(b)), then a small applied voltage $V > V_{th}$ could transmit green light and predominantly diffract red and blue (Fig. 1(c)). At high voltage, the grating profile is effectively 'erased' ($\eta_0(\lambda) \approx 100\%$), and will re-appear when the applied voltage is removed (a feature critical to the other LCPG applications, including displays^{16,17}). Note that even when d is large, the voltage threshold²⁸ can be designed to remain approximately 1-2 V.

The basic fabrication process of an LCPG is fairly simple:^{16,23,26} First, a polarization hologram is created by superimposing two coherent beams from an ultraviolet laser with orthogonal circular polarizations with a small angle between them (easily creating periods $\Lambda > 4\mu\text{m}$). Next, two glass substrates are coated with a photo-alignment material,²⁹ and laminated together such that a uniform thickness (usually a few μm) is achieved. This is then exposed via the polarization hologram capturing the pattern in the photo-alignment layers (Fig. 1(a)).

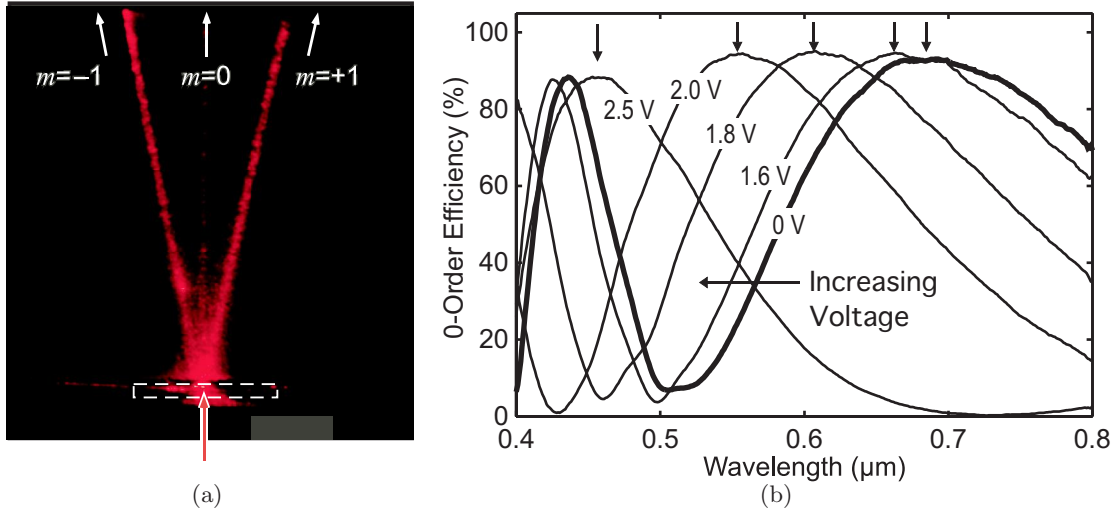


Figure 2. Experimental results from a single LCPG: (a) Photograph of diffraction ($\Lambda = 3 \mu\text{m}$) of HeNe laser (633 nm) light incident with linear polarization; and (b) Transmission spectra of a different sample, with several applied voltages. (color figure)

Finally, a nematic LC fills the gap by capillary action, and the desired LCPG structure is realized as the surfaces direct the LC orientation (Fig. 1(b)).

We generally find excellent agreement between our experimental results and Eq. (1). In Fig. 2(a), a photograph of a HeNe laser being diffracted by an LCPG^{18,19} clearly shows the near-complete coupling into the \pm first-orders. In this case, $\Lambda = 3\mu\text{m}$ and $2\Delta nd \approx 633 \text{ nm}$. In Fig. 2(b), the zero-order spectra of an LCPG is measured at various voltages, showing deep spectral modulation and the blue-shift tuning effect. Note that while the LCPG experiments^{22,26} yielded low diffraction efficiency and high scattering, high quality LCPGs with $\sim 100\%$ efficiency were later reported in switchable^{16,21,30} and polymer^{18,19} LC materials.

The most important design constraint on LCPG fabrication involves a competition between the optical and elastic requirements. Eqs. (1) and (2) determine a required thickness d in order to achieve a transmittance peak at a particular wavelength, given the parameters Δn and N . However, elastic continuum analysis²⁸ with strong anchoring identifies a (best-case) minimum grating period which can be fabricated given the thickness. Combining these two requirements into one constraint leads to

$$\Lambda < \frac{N\lambda_N}{\Delta n} \sqrt{\frac{2K_3}{K_1} - \frac{K_2}{K_1}}, \quad (3)$$

where K_1 , K_2 , and K_3 are the elastic constants corresponding to splay, twist, and bend deformations, respectively. For most LCs, this leads to $\Lambda > 1.5d$, and can be dramatically higher if weak anchoring occurs.²⁸ When this inequality is violated, the director profile $\mathbf{n}(x)$ spontaneously distorts out-of-plane (even without an applied voltage), and defects become much more energetically favorable (degrading optical quality of the PG). Since this constraint enables the desired in-plane profile of LCPGs to manifest accurately, it should be kept in mind throughout the following discussion on tunable optical filters based on LCPGs.

4. THE LCPG TUNABLE OPTICAL FILTER - THEORY AND PROSPECTS

We propose to employ multiple LCPGs as a tunable optical filter in a stacked configuration followed by a spatial-filter (Fig. 3). In this way, we aim to benefit from their high transmittance, polarization-independence, low voltage requirements, and experimentally-demonstrated deep spectral modulation. After first describing the operational concepts and governing equation of the LCPG tunable optical filter, we will describe three possible

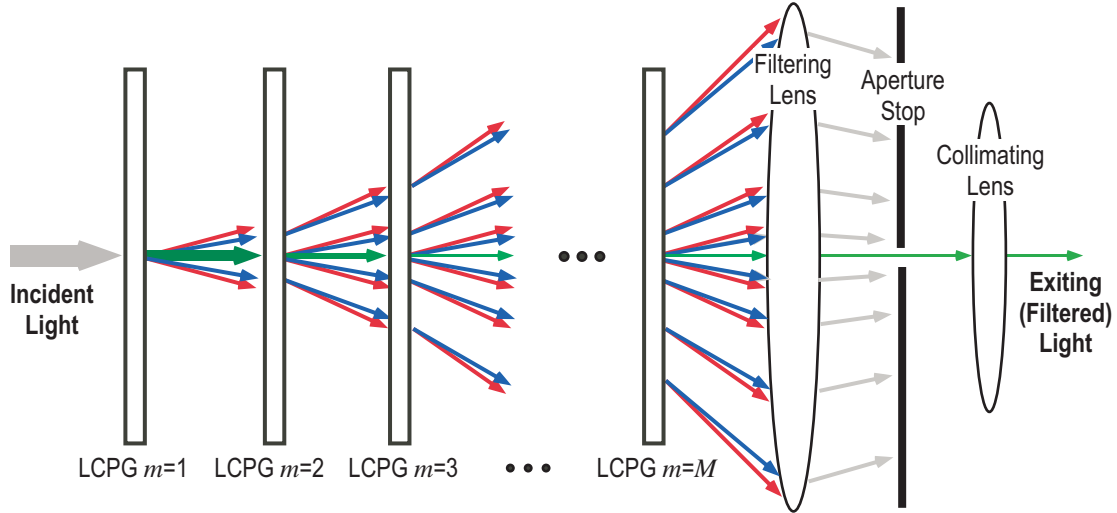


Figure 3. Overall LCPG tunable filter concept, including the M stages of LCPGs and a lens aperture-stop (an elemental spatial filter). Light at wavelengths within the passbands pass directly through the assembly, while all other wavelengths are diffracted away from the optical axis (with an angle governed by the grating equation). (color figure)

configurations and discuss their trade-offs. We will characterize the wavelength bandwidth (full-width at half-maximum - FWHM), the frequency separation between neighboring peaks (free-spectral-range - FSR), and the number of pass-band widths in a spectral period (finesse = FSR/FWHM).

The concept is relatively simple, and is illustrated in a generic way in Fig. 3. We stack three or more LCPGs of potentially different thicknesses and block all but the 0 order using a spatial filter of some kind. The transmittance of the LCPG stack is therefore a multiplication of the individual zero-order efficiencies and the losses due to Fresnel reflections and electrode absorption:

$$T(\lambda) = K^M \prod_{m=1}^M \eta_{0,m}(\lambda) = K^M \prod_{m=1}^M \cos^2 \left(\frac{\pi \Delta n d_m}{\lambda} \right) \quad (4)$$

where M is the total number of stages, K is the combined transmittance of the substrates and electrodes within each stage, $\eta_{0,m}(\lambda)$ is the efficiency of stage m , and d_m is the LC layer thickness of grating m . Keep in mind that it is most accurate to consider $\Delta n \rightarrow \Delta n(V)$, which accomplishes the tuning effect. Given a design wavelength λ_0 and LC material, Eq. (2) can be employed to determine a minimum thickness required by setting $N = 1$. Note that the thinnest LCPG must be at least thick enough to exhibit one full-wave retardation ($\Delta n d_1 \geq \lambda_0$).

There are several design possibilities involving the choice of d_m and M , which have their impact on the primary bandpass filter parameters, particularly FWHM (Fig. 5(a)) and finesse (Fig. 5(b)). The key aspect is that the set of d_m must be chosen so that a peak transmittance occurs in each of the individual LCPG layers at the design wavelength. We identify an exponential, linear, and compound progression of the stage thicknesses, as described below. Example spectra of each are shown in Fig. 4, for the design wavelength $\lambda_0 = 0.6 \mu\text{m}$ and neglecting substrate losses ($K^M = 1$).

As will become apparent, the maximum LC layer thickness required is one of the most important consequences of these configurations, and as with all LC devices, large thicknesses (e.g. $d > 50 \mu\text{m}$) are difficult to work with because they tend to have slow response times and are prone to defects. Furthermore, a larger thickness imposes a large grating period (typically $\Lambda \geq 1.5d$). While this is usually achievable using holographic techniques, a large Λ leads to a small angle separating the zero- and first-orders, and restricts the numerical aperture of the tunable filter. Note that $\text{FSR} = c/\lambda_0$ (where c is the vacuum speed of light) for all three of these LCPG filter configurations.

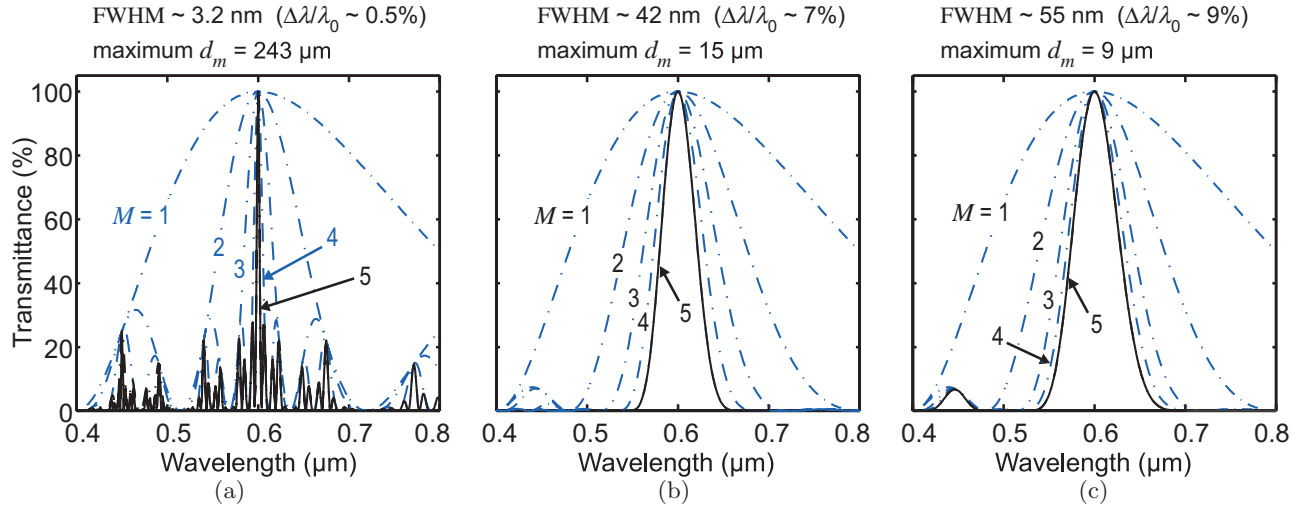


Figure 4. Calculated transmission spectra of three possible LCPG optical filter configurations ($M = 5$), distinguished by the progression of thicknesses of each stage: (a) Exponential; (b) Linear; and (c) Compound. Note the inherent trade-off between FWHM and maximum required stage thickness. (color figure)

4.1 Stage Design: Exponential Progression

One of the more obvious options is to set $d_m = d_0 2^{(m-1)}$ (an exponential progression), which is analogous to the conventional Lyot filter (but which does not suffer from the polarization losses):

$$T_{exp}(\lambda) = K^M \prod_{m=1}^M \cos^2 \left(\frac{\pi \Delta n d_0}{\lambda} 2^{m-1} \right). \quad (5)$$

An example of this filter is shown in Fig. 4(a), showing the spectra for $M = 1$ to 5. This design has an advantage in that it manifests the best FWHM and finesse (Fig. 5) for any given M of the options discussed here, but requires the largest grating thickness (Fig. 5(c)). Because large LCPG thicknesses are generally undesirable (which usually occurs even for $M > 5$), the following alternative options are expected to be more realistically implemented.

4.2 Stage Design: Linear Progression

A second option is to set $d_m = d_0 m$ (a linear progression):

$$T_{lin}(\lambda) = K^M \prod_{m=1}^M \cos^2 \left(\frac{\pi \Delta n d_0}{\lambda} m \right). \quad (6)$$

Example spectra of this filter are shown in Fig. 4(b), for $M \leq 5$. In this case, the maximum thickness necessary for a desired FWHM (and finesse) is slightly lower (Fig. 5(c)), at the expense of requiring more stages.

4.3 Stage Design: Compound Progression

The third option we identify is a compound filter where the linear progression ($d_m = d_0 m$) is used for the first M_0 stages (up to a certain thickness), after which the highest thickness with ($d_m = d_0 M_0$) is subsequently repeated M_1 times. The transmittance in this case follows

$$T_{comp}(\lambda) = K^{M_0+M_1} \cos^{2M_1} \left(\frac{\pi \Delta n d_0}{\lambda} M_0 \right) \prod_{m=1}^{M_0} \cos^2 \left(\frac{\pi \Delta n d_0}{\lambda} m \right). \quad (7)$$

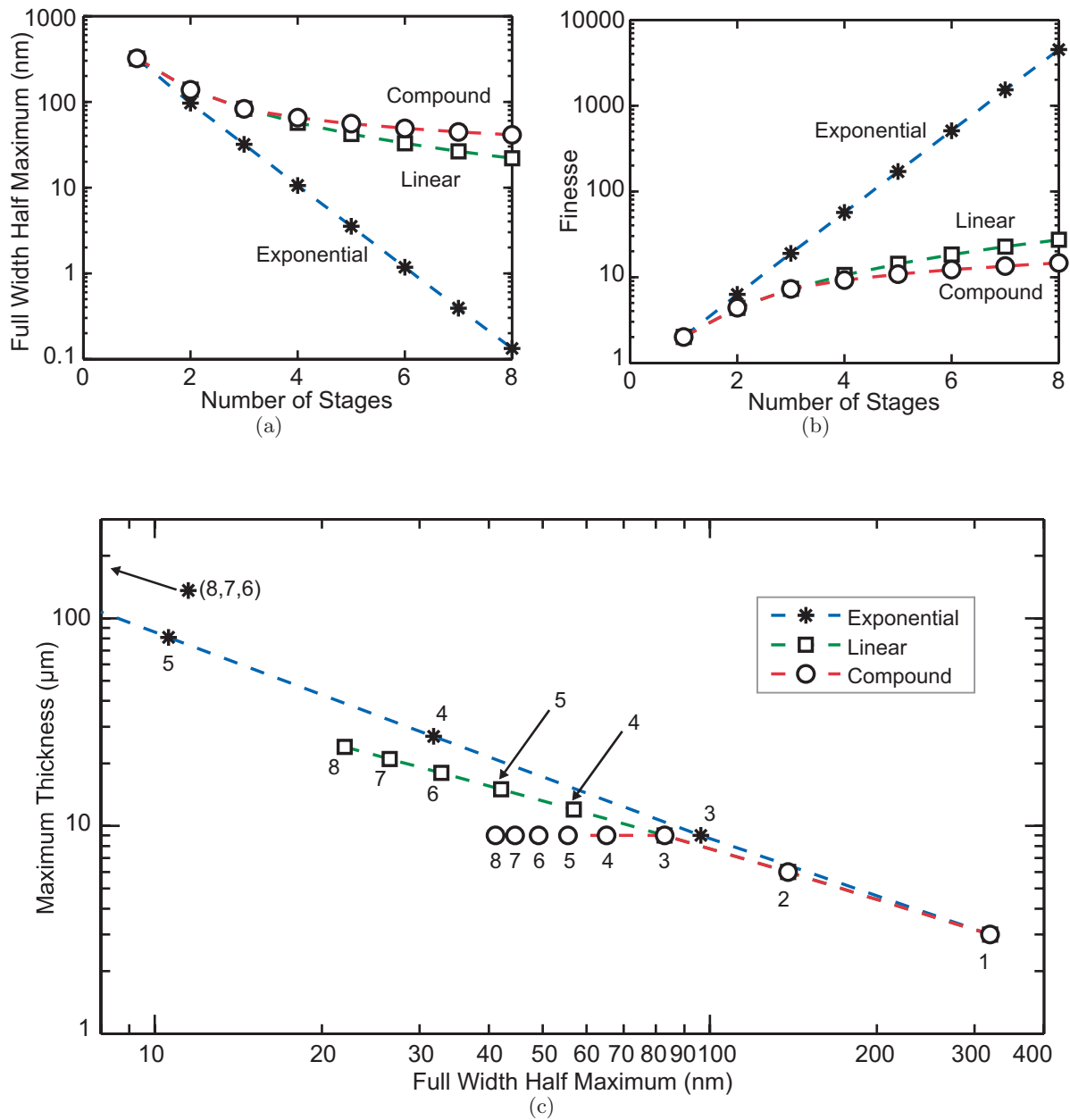


Figure 5. Calculated characteristics of LCPG optical filters versus number of stages M : (a) Full-width at half-maximum (FWHM); (b) Finesse; and (c) Maximum required LCPG thickness and FWHM (numbers indicate M for each point). (color figure)

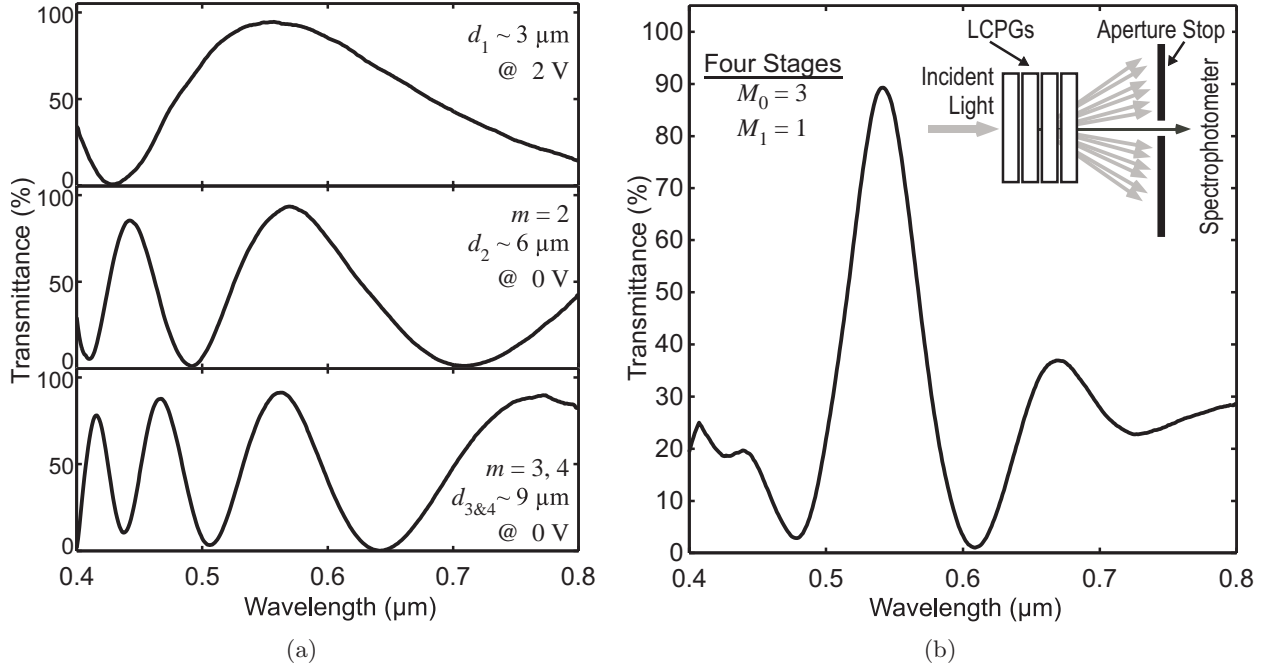


Figure 6. Measured spectra of a LCPG tunable optical filter with a compound progression ($M_0 = 3$ and $M_1 = 1$): (a) Individual spectra of each stage; and (b) Total spectrum of the four laminated stages (optically coupled together with glue). Note that stages 3 and 4 have the same nominal thicknesses.

Example spectra for $M = M_1 + M_0 \leq 5$ and $M_0 = 3$ are shown in Fig. 4(b). The maximum thickness for a given FWHM (and finesse) is even lower than before (Fig. 5(c)), again with the trade-off that more filter stages are required for a desired FWHM.

In addition to the design constraint to limit the maximum d , it is also important to recognize the impact of the term K^M , which would adversely effect the peak transmittance due to the inherent losses at the glass interfaces and electrode absorption. In the following section, we report our first attempts to reduce these ideas to practice by fabricating four LCPGs and implementing the tunable optical filter.

5. PRELIMINARY RESULTS

We constructed a four-stage LCPG tunable optical filter with a compound progression ($M_0 = 3$ and $M_1 = 1$). We utilized a nematic LC MLC-6080 (Merck, $\Delta n = 0.202$ at 589 nm, $T_{NI} = 95^\circ\text{C}$) and chose a design wavelength $\lambda_0 = 0.56 \mu\text{m}$. Note that in fabrication,^{16,26} we additionally used photo-alignment material ROP-103/CP2, and a holographic exposure dose around $0.3 \text{ J}\cdot\text{cm}^{-2}$. Following Eq. (2), we must reach $d_1 > \lambda_0/\Delta n = 2.8 \mu\text{m}$.

We therefore chose to use nominal thicknesses of $d_1 = 3 \mu\text{m}$ (one wave retardation), $d_2 = 6 \mu\text{m}$ (two wave retardation), and $d_3 = d_4 = 9 \mu\text{m}$ (three wave retardation). These thicknesses were attained using silica spheres of these sizes dispersed in the glue seal of the LCPG. The individual transmission spectra at each thickness is shown in Fig. 6(a), referenced to an ITO cell filled with an isotropic dielectric (glue). Each of these spectra have a high transmission fringe around λ_0 , as designed. Notice that the peak transmission for most spectral fringes are near 100% and that the minima are near 0%, corresponding well to theory. Note that all spectra shown here are measured using collimated unpolarized light in the configuration illustrated in the inset of Fig. 6(b), using a conventional bench-top spectrophotometer (Varian CARY 5E). The aperture stop was simply a thin aluminum plate with a 2 mm x 5 mm hole.

The transmission spectra of the LCPG tunable filter that results when we laminate the four stages together is shown in Fig. 6(b), where we applied and cured optical adhesive in between each stage (to minimize Fresnel reflection losses). As predicted, a bandpass filter notch appears at $\lambda_0 = 0.56 \mu\text{m}$, with high peak transmittance

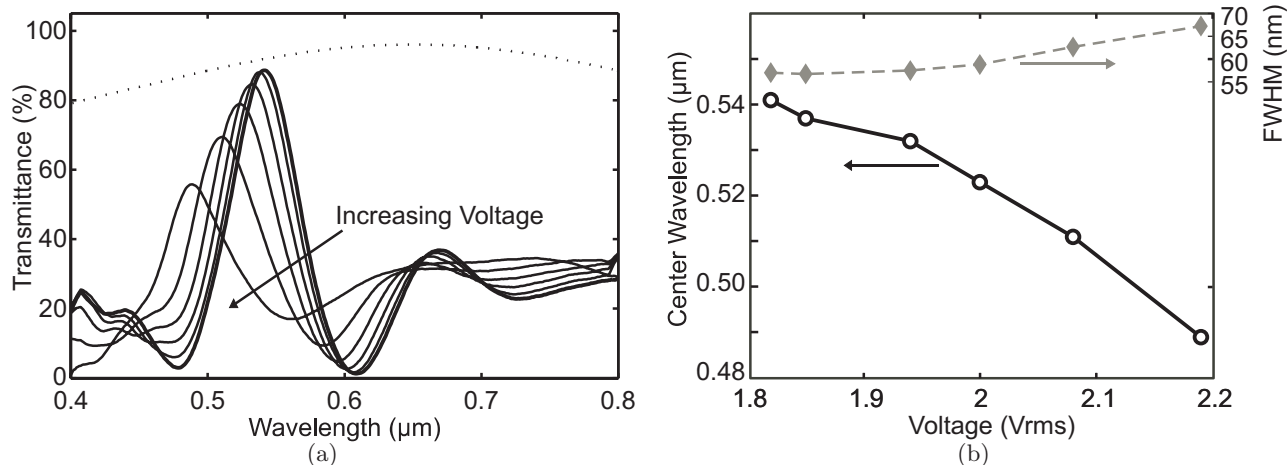


Figure 7. Electrical tuning characteristics of a four-stage LCPG optical filter: (a) Transmission spectra for various voltages (1.82 V, 1.85 V, 1.94 V, 2.00 V, 2.08 V, and 2.19 V); and (b) Voltage response of the bandpass center wavelength and FWHM. Note that the dotted line in part (a) is a reference spectra including the substrate absorption and interface losses, obtained as an assembly of four stages filled only with glue.

($\sim 88\%$), substantially higher than almost any tunable optical filter approach using polarizers. We also observe a minimum FWHM (57 nm) close to that predicted (68 nm) by analyzing Eq. (7). Note that the analysis in Section 4 did not include the effect of chromatic dispersion of in the LC, but its effect is likely to reduce the FWHM (as seen in this example). We also notice that an undesirable sidelobe is persistent at around $0.68 \mu\text{m}$, whose origins we are unable to explain at the moment.

To electrically tune the filter and obtain the best possible characteristics, each stage must be individually controlled by an applied voltage. To begin with, each stage is biased such that its operational fringe occurs at λ_0 . This may require a slightly different voltage (in the range of 1-2 V) for each stage because of small fabrication differences. This ‘calibration’ results in a single bandpass region with maximum peak transmittance and minimum FWHM (as was done for the result in Fig. 6(b)). Then, this peak can be tuned across a wide wavelength range by increasing the voltage applied to the filter while maintaining the same voltage ratio among the individual cells (an action easily accomplished using simple voltage dividers).

The electrical tuning characteristics of this LCPG optical filter are shown in Fig. 7. The voltage-resolved spectra are shown in Fig. 7(a), where we notice that the notch persists even over a modest tuning range (540 nm to 480 nm is $\sim 10\%$ of the starting wavelength), and that low voltages (< 2.2 V) are needed. The central wavelength of the bandpass peak and the FWHM for each tuning voltage are shown in Fig. 7(b). While the essential tuning function is clearly prominent, we notice two degrading effects as the voltage is applied: a reduction in the peak transmittance (from 88% to 55%) and an increase in the FWHM (from 57 nm to ~ 67 nm). We are uncertain as to the origins of these effects, but anticipate that these are related to our current preliminary driving scheme and non-ideal fabrication (and not a fundamental limitation).

In order to improve our current results, we suggest first the addition of more stages to the filter. As evidenced in Fig. 5, for any of the suggested configurations the FWHM decreases as the number of stages increases. We must further optimize materials and fabrication to improve these maximum thicknesses. We also acknowledge that a careful study is needed regarding the characteristics of the bandpass including the reason for the decreased peak transmittance and increased FWHM at lower wavelengths as well as the existence of the secondary sidelobe visible in the spectrum.

6. CONCLUSION

We have experimentally demonstrated a LCPG tunable optical filter with a peak transmittance of 88%, a FWHM of ~ 60 nm, a tuning range of 540 nm to 480 nm, and low drive voltages (< 2.2 V). So far as we are aware, we

introduce the device concept, theory, and validation for the first time. Most critically, this has been implemented with a polarization-independent approach without polarizers, and uses materials and construction with strong potential for low cost and small size implementations. We also derive the theoretical expressions that govern the design of LCPG optical filters in general, and discuss the available options and their trade-offs to yield higher quality passbands (in FWHM and finesse). We conclude that the LCPG tunable optical filter shows properties ideal for use in compact, portable spectrometers and other low cost remote sensing systems.

ACKNOWLEDGMENTS

The authors gratefully acknowledge financial support from the National Science Foundation (grant ECCS-0621906). The authors also thank Sai Fu for assistance with early experimental fabrication and theoretical studies.

REFERENCES

1. B. Lyot, "Filter monochromatique polarisane et ses applications en physique solarie," *Annales d'Astrophysique* **7**, p. 31, 1944.
2. C. Ye, "Low-loss tunable filter based on optical rotatory dispersion," *Applied Optics* **45**(6), pp. 1162–1168, 2006.
3. I. Solc, "Birefringent chain filters," *Journal of the Optical Society of America* **55**(6), pp. 621–625, 1965.
4. B. Benkelfat, Q. Zout, and B. Vonouze, "Low-voltage continuous tunable hybrid filter for tailored optical-bandwidth operation," *IEEE Photonics Technology Letters* **16**(4), pp. 1098–1100, 2004.
5. J. Evans, "Solc birefringent filter," *Journal of the Optical Society of America* **48**(3), pp. 142–145, 1958.
6. X. Xia, J. Stockley, T. Ewing, and S. Serati, "Advances in polarization-based liquid crystal optical filters," *Proceedings of SPIE* **4658**, pp. 51–58, 2002.
7. J. Evans, "The birefringent filter," *Journal of the Optical Society of America* **39**(3), pp. 229–242, 1949.
8. M. Datta, M. Pruessner, D. Kelly, and R. Ghodssi, "Design of MEMS-tunable novel monolithic optical filters in InP with horizontal Bragg mirrors," *Solid-State Electronics* **48**(10-11), pp. 1959–1963, 2004.
9. C. Chen, C. Pan, C. Hsieh, Y. Lin, and R. Pan, "Liquid-crystal-based terahertz tunable Lyot filter," *Applied Physics Letters* **88**(10), pp. 101–107, 2006.
10. A. Sneh and K. Johnson, "High-speed continuously tunable liquid crystal filter for WDM networks," *Journal of Lightwave Technology* **14**(6), pp. 1067–1080, 1996.
11. K. Hirabayashi and T. Kurokawa, "A tunable polarization-independent liquid crystal Fabry-Perot interferometer filter," *IEEE Photonics Technology Letters* **4**(7), pp. 740–742, 1992.
12. H. Xianyu, S. Faris, and G. Crawford, "In-plane switching of cholesteric liquid crystals for visible and near-infrared applications," *Applied Optics* **43**(26), pp. 5006–5015, 2004.
13. J. W. McMurdy, G. P. Crawford, and G. D. Jay, "Monolithic microspectrometer using tunable ferroelectric liquid crystals," *Applied Physics Letters* **89**(081105), 2006.
14. J. W. McMurdy, J. N. Eakin, and G. P. Crawford, "Vertically aligned deformed helix ferroelectric liquid crystal configuration for reflective display device," *SID Symposium Digest* **37**, pp. 677–680, 2006.
15. E. Nicolescu and M. J. Escuti, "Compact spectrophotometer using polarization-independent liquid crystal tunable optical filters," *Proceedings of SPIE* **6661**, p. no.4, 2007.
16. M. J. Escuti and W. M. Jones, "A polarization-independent liquid crystal spatial-light-modulator," *Proceedings of SPIE* **6332**, p. 633222, 2006.
17. W. M. Jones, B. L. Conover, and M. J. Escuti, "Evaluation of projection schemes for the liquid crystal polarization grating operating on unpolarized light," *SID Symposium Digest* **37**, pp. 1015–1018, 2006.
18. M. J. Escuti, C. Oh, C. Sanchez, C. W. M. Bastiaansen, and D. J. Broer, "Simplified spectropolarimetry using reactive mesogen polarization gratings," *Proceedings of SPIE* **6302**, p. 630207, 2006.
19. M. J. Escuti, C. Oh, C. van Heesch, C. Sanchez, C. W. M. Bastiaansen, and D. J. Broer, "Reactive mesogen polarization gratings with small pitch and ideal properties," *Advanced Materials*, p. submitted for publication, 2007.

20. G. Crawford, J. Eakin, M. Radcliffe, A. Callan-Jones, and R. Pelcovits, "Liquid-crystal diffraction gratings using polarization holography alignment techniques," *Journal of Applied Physics* **98**, p. 123102, 2005.
21. C. Provenzano, P. Pagliusi, and G. Cipparrone, "Highly efficient liquid crystal based diffraction grating induced by polarization holograms at the aligning surfaces," *Applied Physics Letters* **89**, p. 121105, 2006.
22. H. Sarkissian, S. V. Serak, N. Tabirian, L. B. Glebov, V. Rotar, and B. Y. Zeldovich, "Polarization-controlled switching between diffraction orders in transverse-periodically aligned nematic liquid crystals," *Optics Letters* **31**(15), pp. 2248–2250, 2006.
23. L. Nikolova and T. Todorov, "Diffraction efficiency and selectivity of polarization holographic recording," *Optica Acta* **31**, pp. 579–588, 1984.
24. J. Tervo and J. Turunen, "Paraxial-domain diffractive elements with 100% efficiency based on polarization gratings," *Optics Letters* **25**(11), pp. 785–786, 2000.
25. F. Gori, "Measuring stokes parameters by means of a polarization grating," *Optics Letters* **24**(9), pp. 584–586, 1999.
26. J. Eakin, Y. Xie, R. Pelcovits, M. D. Radcliffe, and G. Crawford, "Zero voltage freedericksz transition in periodically aligned liquid crystals," *Applied Physics Letters* **85**(10), pp. 1671–1673, 2004.
27. C. Oh and M. J. Escuti, "Numerical analysis of polarization gratings using the finite-difference time-domain method," *Physical Review A* **76**, p. in press, 2007.
28. R. Komanduri and M. J. Escuti, "Elastic continuum analysis of the liquid crystal polarization grating," *Physical Review E* **76**, p. in press, 2007.
29. M. Schadt, H. Seiberle, and A. Schuster, "Optical patterning of multi-domain liquid-crystal displays with wide viewing angles," *Nature* **381**, pp. 212–215, 1996.
30. M. J. Escuti and W. M. Jones, "Polarization independent switching with high contrast from a liquid crystal polarization grating," *SID Symposium Digest* **37**, pp. 1443–1446, 2006.